

# Singularity and universality from von Neumann to Rényi entanglement entropy and disorder operator in Motzkin chains

Jianyu Wang,<sup>1,2,3,4,5</sup> Zenan Liu,<sup>6,5</sup> Zheng Yan,<sup>6,5,\*</sup> and Congjun Wu<sup>2,3,4,5,†</sup>

<sup>1</sup>*State Key Laboratory of Surface Physics and Department of Physics, Fudan University, Shanghai 200438, China*

<sup>2</sup>*New Cornerstone Science Laboratory, Department of Physics,  
School of Science, Westlake University, Hangzhou 310024, China*

<sup>3</sup>*Institute for Theoretical Sciences, Westlake University, Hangzhou 310024, China*

<sup>4</sup>*Key Laboratory for Quantum Materials of Zhejiang Province,  
School of Science, Westlake University, Hangzhou 310024, China*

<sup>5</sup>*Institute of Natural Sciences, Westlake Institute for Advanced Study, Hangzhou 310024, China*

<sup>6</sup>*Department of Physics, School of Science and Research Center for  
Industries of the Future, Westlake University, Hangzhou 310030, China*

(Dated: January 31, 2025)

The Rényi entanglement entropy is widely used in studying quantum entanglement properties in strongly correlated systems, whose analytic continuation as  $n \rightarrow 1$  is often believed to give rise to the celebrated von Neumann entanglement entropy. However, this process for the colored Motzkin spin chain exhibits a singularity that yields different scaling behaviors of  $\sim \sqrt{l}$  and  $\sim \log l$  for the von Neumann and Rényi entropies, respectively. It can be understood by the exponential increasing density of states in its entanglement spectrum. We have also employed disorder operators under various symmetries to study such a system. The analytical and numerical results reveal that the scaling of disorder operators is also  $\log l$  in the leading term, the same as the Rényi entanglement entropy. We propose that the coefficient of the term  $\log l$  is a universal constant, both in Rényi entropies and disorder operators, which could be used to identify the constraint physics of Motzkin walks.

## I. INTRODUCTION

In recent years, the interflow and mutual learning between condensed matter and quantum information have inspired increasingly fruitful research [1–3]. In the field of quantum information, the entanglement entropy (EE) plays a key role in measuring the amount of information and chaos [4, 5]. As one of the basic properties of quantum mechanics, the measurement of quantum entanglement itself is a fundamental problem. Moreover, the introduction of EE in condensed matter physics has revealed richer physics, such as topological entanglement entropy and long-range entanglement in highly entangled matter [6, 7]. One important topic in condensed matter is using EE to probe the intrinsic physics of many-body systems [6–10]. Among many intriguing features, EE offers a direct connection between conformal field theory (CFT) and categorical description of the problems beyond traditional observables [11–27].

Unlike in few-body systems, the scaling behaviors of EE in quantum many-body systems always reveal universal physics, such as central charge [11, 28, 29], the number of Goldstone modes [30–33], and the quantum dimension of topological order [6, 7, 24, 34]. With the development of CFT [15, 35–38], we are aware that the EE with corner cutting in two-dimensional quantum systems usu-

ally obeys the area-law behaviors  $s = al + b \ln l + \gamma$ , where  $S$  is the EE and  $l$  is the length of the entangled boundary, in which the coefficient  $b$  is related to the angular of corners and  $a$  is generally thought as UV dependent. Meanwhile, the coefficients  $b$  and  $\gamma$  usually can extract universal information and be used to detect novel phases and criticalities [2].

The von Neumann (VN) EE  $s_A^{\text{VN}} = -\text{Tr}(\rho_A \log \rho_A)$  ( $\rho_A$  is the reduced density matrix) as the generalization of the Shannon entropy in quantum mechanics is widely used in exploring the above questions [39–42]. However, due to the difficulty in the calculation of the VN EE, Rényi EE is much more commonly used both in field theory and numeric. The definition of Rényi EE is  $s_A^{(n)} = \frac{1}{1-n} \log[\text{Tr}(\rho_A^n)]$ , where  $n$  is Rényi index. Formally, the Rényi EE will become back to VN EE when  $n \rightarrow 1$ . The form of Rényi EE does not contain the logarithm operator for a matrix which is friendly for either analytical or numerical calculations. Although the Rényi EE loses some properties in additivity and sub-additivity [43–47], it is strongly believed to have the same scaling behaviors, such as area law and volume law, as the VN EE. It demonstrates in the past that all the coefficients of the VN EE for each  $O(l)$  term can be obtained via the analytic continuation of the Rényi index. In a large number of examples within field theory and numerical results, the good belief has been massively validated [48, 49].

Does the analytic continuation from Rényi EE to VN EE always work? To answer this long-standing question, we systematically study the VN and Rényi EE scaling

\* zhengyan@westlake.edu.cn

† wucongjun@westlake.edu.cn

behaviors of a 1D colored Motzkin spin chain with different spin  $S$  analytically and numerically. We find that there is a singularity in the limit of Rényi index  $n \rightarrow 1$ , in which the coefficient of the leading term  $\log l$  will be divergent. It actually indicates that an extra term  $\sqrt{l}$  becomes the leading term in the VN EE. This result provides a counter-example for the analytic continuation from Rényi to von Neumann EE, which cautions people should be careful in the EE studies.

Meanwhile, the disorder operator (DO) is a non-local observable, similar to the EE, which is proposed to extract the high-form symmetry and CFT information of quantum many-body systems [50–53]. It has been successfully used to detect the high-form symmetry breaking at Ising transition [54]. The current central charge can be captured from the DO at (2+1)D  $O(2)$  and  $O(3)$  phase transition in the CFT [55, 56]. Fermion DOs are also designed to explore the universal feature of Fermi liquid, Luttinger liquid, and fermion QCP and reflect the non-unitary conformal field theory (CFT) of fermion DQCP [57–59]. The DO satisfies the universal scaling behaviors, where the logarithmic term usually reflects the general feature of CFT at the conformal invariant QCP. In this Motzkin chain, we also investigate the scaling behaviors of DO, whose scaling behaviors are similar to the Rényi EE. Moreover, we find that the coefficient of the logarithmic term is universal for any spin value, regardless of whether it is in DO or EE. It can help us identify the system of Motzkin walks.

## II. BACKGROUND OF MOTZKIN CHAINS

Consider random walks starting from the point  $(0, 0)$  and ending at  $(2l, 0)$  on the  $x-y$  plane as shown in Fig. 1. These walks consist of three types of steps: upward steps  $/$ , downward steps  $\backslash$ , and horizontal steps  $-$ , represented as vectors  $(1, 1)$ ,  $(1, -1)$  and  $(1, 0)$ , respectively. Then Motzkin walks are defined as those random walks that do not cross below the  $x$ -axis. Bravyi et al. [60] introduced a frustrated-free spin-1 chain model whose unique ground state is the superposition of all Motzkin walks states, achieved by mapping the spin  $S^z$  states  $\{\uparrow, 0, \downarrow\}$  to the steps  $\{/, -, \backslash\}$ , respectively. Movassagh and Shor [61] then generalized this model into an  $S$ -colored Motzkin model, where the upward or downward steps are colored using  $S$  different colors. This model can be translated to a spin- $S$  quantum chain. An example of the 2-colored Motzkin walk is shown in Fig. 1. For a  $S$ -colored Motzkin model of size  $2l$ , the Hamiltonian is constructed by local projection operators and has the form:

$$H = \Pi^{\text{boundary}} + \sum_{j=1}^{2l-1} \Pi_{j,j+1}^{\text{cross}} + \sum_{j=1}^{2l-1} \Pi_{j,j+1}^{\text{exchange}}, \quad (1)$$

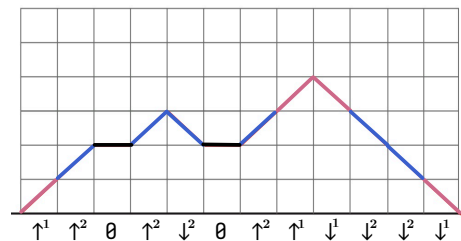


FIG. 1. Example of a 2-colored Motzkin walk (colored path). The walk starts and ends on the  $x$ -axis, and cannot cross below it. It can be mapped to a  $S^z$  configuration of a spin-2 chain. In this figure, the pink upward and downward steps are mapped to  $S^z = \pm 1$ , the blue steps are mapped to  $S^z = \pm 2$ , and the black horizontal steps are mapped to  $S^z = 0$ .

in which

$$\begin{aligned} \Pi^{\text{boundary}} &= \sum_{k=1}^S (|\downarrow^k\rangle_1 \langle \downarrow^k| + |\uparrow^k\rangle_{2l} \langle \uparrow^k|), \\ \Pi_{j,j+1}^{\text{cross}} &= \sum_{k \neq k'}^S |\uparrow^k \downarrow^{k'}\rangle_{j,j+1} \langle \uparrow^k \downarrow^{k'}|, \\ \Pi_{j,j+1}^{\text{exchange}} &= \sum_{k=1}^S (|D^k\rangle_{j,j+1} \langle D^k| + |U^k\rangle_{j,j+1} \langle U^k| \\ &\quad + |V^k\rangle_{j,j+1} \langle V^k|), \end{aligned} \quad (2)$$

where the superscript  $k$  indicate colors, i.e.  $\uparrow^k$  stands for  $S^z = k$  state and  $\downarrow^k$  stands for  $S^z = -k$  state. The boundary term ensures that the first and last steps will not pass below the  $x$ -axis. The cross term keeps the correct order of different color pairs. As a counter-example,  $\uparrow^k \uparrow^{k'} \downarrow^k \downarrow^{k'}$  is not allowed if  $k \neq k'$ . And the exchange term contains states  $|D^k\rangle = |\downarrow^k 0\rangle - |0 \downarrow^k\rangle$ ,  $|U^k\rangle = |\uparrow^k 0\rangle - |0 \uparrow^k\rangle$  and  $|V^k\rangle = |\uparrow^k \downarrow^k\rangle - |00\rangle$ , which leads to the steps exchanging of

$$\swarrow \leftrightarrow \searrow, \quad \searrow \leftrightarrow \swarrow, \quad \wedge \leftrightarrow \_ . \quad (3)$$

Notice that there is no such step exchange as

$$\swarrow \leftrightarrow \_ , \quad (4)$$

and this property ensures that the walk height remains positive. The ground state of the Hamiltonian (1) is the superposition of all the Motzkin walk configurations  $|M_i\rangle$ ,

$$|G\rangle = \frac{1}{\sqrt{N}} \sum_i^N |M_i\rangle, \quad (5)$$

where  $N$  is the number of all the Motzkin walks allowed.

## III. THE ANALYTIC SOLUTION OF EE

We firstly investigate the EE  $s_l$  of half-cutting on a  $S$ -colored Motzkin chain with size length  $2l$ . The VN EE

( $n \rightarrow 1$ ) takes the form as

$$\begin{aligned} s^{\text{VN}} &= a\sqrt{l} + b \log l + \text{const.} \\ a &= 2 \log S \sqrt{\frac{2\sqrt{S}}{(2\sqrt{S}+1)\pi}} \\ b &= \frac{1}{2} \end{aligned} \quad (6)$$

and the Rényi EE ( $n > 1$ ) takes the form as

$$\begin{aligned} s^{(n)} &= b \log l + \text{const.}, \\ b &= \frac{3}{2} \left(1 + \frac{1}{n-1}\right). \end{aligned} \quad (7)$$

These equations hold for all the colored case [61, 62]. For comparison, when  $S = 1$  the leading terms of both the VN EE and Rényi EE are  $\frac{1}{2} \log l$ . As a notation, the log in this article stands for the natural logarithm.

The analytical results reveal that there is a singularity at  $n = 1$ , which leads to different scaling behaviors of VN EE and Rényi EE. The details of the analytical calculations are provided below. The ground state of a  $S$ -colored Motzkin chain has been previously described equation (5). Cutting at the midpoint and tracing out half of the chain, the reduced density matrix is  $\rho_l = \text{Tr}_l |G\rangle \langle G|$ , whose eigenvalues are [61]

$$\lambda_m = \frac{S^{-m}}{T} \frac{m^2}{l} \exp \left[ -\frac{1}{2} \left(2 + \frac{1}{\sqrt{S}}\right) \frac{m^2}{l} \right], \quad (8)$$

where the degeneracy of  $\lambda_m$  is  $S^m$ . Here  $T$  is a normalized factor such as  $\sum_m S^m \lambda_m = 1$ . The  $n$ -th Rényi EE is then given by

$$s^{(n)} = \frac{1}{1-n} \log \sum_{m=0}^l S^m \lambda_m^n. \quad (9)$$

Substituting  $m$  with  $\xi = m/\sqrt{l}$  and using the integral approximation, the Rényi EE is expressed as then

$$\begin{aligned} s^{(n)} &\simeq \frac{1}{2} \log l + \frac{1}{1-n} \log \tilde{T}^{-n} \int_0^{\sqrt{l}} d\xi \xi^{2n} \times \\ &\exp \left[ -\frac{n}{2} \left(2 + \frac{1}{\sqrt{S}}\right) \xi^2 - (n-1) \log(S) \sqrt{l} \xi \right], \end{aligned} \quad (10)$$

where

$$\tilde{T} = \frac{T}{\sqrt{l}} \simeq \int_0^{\sqrt{l}} d\xi \xi^2 \exp \left[ -\frac{1}{2} \left(2 + \frac{1}{\sqrt{S}}\right) \xi^2 \right]. \quad (11)$$

For the case  $n > 1$ , the Rényi EE can be simplified to

$$s^{(n)} = \frac{1}{2} \log l - \frac{n}{1-n} \log \tilde{T} + s_3^{(n)}, \quad (12)$$

where

$$\begin{aligned} s_3^{(n)} &= \frac{1}{1-n} \log \int_0^{\sqrt{l}} d\xi \xi^{2n} \exp \left[ -\frac{n}{2} \left(2 + \frac{1}{\sqrt{S}}\right) \xi^2 \right. \\ &\left. - (n-1) \log(S) \sqrt{l} \xi \right]. \end{aligned} \quad (13)$$

For convenience, let us define the following functions:

- Define functions  $p_1$  and  $p_2$  as

$$\begin{aligned} p_1(n, S) &= \frac{n}{2} \left(2 + \frac{1}{\sqrt{S}}\right), \\ p_2(n, S) &= (n-1) \log(S). \end{aligned} \quad (14)$$

- Define function  $f_\alpha$  as

$$f_\alpha(l) = l^{\alpha/2} \exp[-(p_1 + p_2)l]. \quad (15)$$

- Define function  $F_\alpha$  as

$$\begin{aligned} F_\alpha(p_1, p_2, l) &= \\ &\int_0^{\sqrt{l}} d\xi \xi^\alpha \exp \left[ -p_1(n, S) \xi^2 - p_2(n, S) \sqrt{l} \xi \right]. \end{aligned} \quad (16)$$

Consequently, the function  $\tilde{T}$  in (11) can be expressed as

$$\tilde{T} = F_2(p_1(1, S), 0, l), \quad (17)$$

and  $s_3^{(n)}$ , defined in (13), can be expressed as

$$s_3^{(n)} = \frac{1}{1-n} \log F_{2n}. \quad (18)$$

Obviously,  $F_\alpha$  is positive, and we have the limit  $\lim_{l \rightarrow \infty} F_\alpha \rightarrow 0$ . Additionally, we can easily establish the following relations:

$$\frac{d}{dl} F_\alpha = -\frac{p_2}{2\sqrt{l}} F_{\alpha+1} + \frac{1}{2\sqrt{l}} f_\alpha(l), \quad (19)$$

$$(\alpha+1)F_\alpha = p_2 \sqrt{l} F_{\alpha+1} + 2p_1 F_{\alpha+2} + f_\alpha(l). \quad (20)$$

Because  $F_\alpha$  and  $f$  are the positive, and  $p_2$  is also positive for the condition  $n, S > 1$ , the following limit can be proved according to equation (20):

$$\begin{aligned} \lim_{l \rightarrow \infty} \frac{F_\alpha}{F_{\alpha+1}} &> \lim_{l \rightarrow \infty} \frac{p_2 \sqrt{l}}{\alpha+1} = +\infty, \\ \lim_{l \rightarrow \infty} \frac{f_\alpha(l)}{F_{\alpha+1}} &= 0. \end{aligned} \quad (21)$$

Thus for large enough  $l$  we have the relation

$$F_\alpha \simeq \frac{p_2 \sqrt{l}}{\alpha+1} F_{\alpha+1}. \quad (22)$$

Now we can analyze the scaling of Rényi EE in (12). The first term contributes a logarithmic scaling obviously. The second term contributes a constant because  $\tilde{T}$  has a upper bound in the limit  $l \rightarrow \infty$ , which is

$$\lim_{l \rightarrow \infty} \tilde{T} = \sqrt{\frac{\pi}{2}} \left(2 + \frac{1}{\sqrt{S}}\right)^{-3/2}. \quad (23)$$

Then only the third term  $s_3^{(n)}$  is needed to be calculated. In the following paragraphs, we will prove that the scaling of term  $s_3^{(n)}$  is logarithmic. The exact form of Rényi EE at the large  $l$  limit will also be given.

### A. The logarithmic scaling of $s_3^{(n)}$

We aim to demonstrate that there exists a finite limit for  $s_3^{(n)}$  divided by  $\log l$  as  $l$  approaches infinity:

$$\lim_{l \rightarrow \infty} \frac{s_3^{(n)}}{\log(l)}. \quad (24)$$

Submitting (16) and (15) into (24) and using the L'Hôpital's rule, we obtain:

$$\begin{aligned} & \lim_{l \rightarrow \infty} \frac{s_3^{(n)}}{\log(l)} \\ &= \frac{2n+1}{2n-2} \lim_{l \rightarrow \infty} \frac{p_2 \sqrt{l} F_{2n+1}}{p_2 \sqrt{l} F_{2n+1} + p_1 F_{2n+2}}. \end{aligned} \quad (25)$$

Based on the relation in (22), we have demonstrated that

$$\lim_{l \rightarrow \infty} \frac{s_3^{(n)}}{\log(l)} = \frac{2n+1}{2n-2}. \quad (26)$$

This indicates that the scaling of the  $s_3^{(n)}$  is given by

$$s_3^{(n)} = \frac{2n+1}{2n-2} \log l + \text{const}. \quad (27)$$

### B. The scaling form of Rényi EE

The constant term in the scaling of  $s_3^{(n)}$  is given by

$$\begin{aligned} & \lim_{l \rightarrow \infty} \left( s_3^{(n)} - \frac{2n+1}{2n-2} \log l \right) \\ &= \frac{1}{1-n} \lim_{l \rightarrow \infty} \log \left( l^{\frac{2n+1}{2}} F_{2n} \right). \end{aligned} \quad (28)$$

According to equation (22), the limit of the term in the logarithm function is

$$\begin{aligned} \lim_{l \rightarrow \infty} l^{\frac{2n+1}{2}} F_{2n} &= \frac{\Gamma(2n+1)}{p_2^{2n}} \lim_{l \rightarrow \infty} \sqrt{l} F_0 \\ &= \frac{\Gamma(2n+1)}{p_2^{2n}} \lim_{l \rightarrow \infty} \left( \frac{1}{p_2} - \frac{2p_1}{p_2} F_1 \right) \\ &= \frac{\Gamma(2n+1)}{p_2^{2n+1}}, \end{aligned} \quad (29)$$

where  $\Gamma$  is the gamma function. Thus the constant term in  $s_3^{(n)}$  is

$$\frac{1}{1-n} \log \left( \frac{\Gamma(2n+1)}{p_2^{2n+1}} \right). \quad (30)$$

In summary, substituting (23), (26) and (29) into (13), the expression of Rényi EE (for  $n > 1$  and  $S > 1$ ) is

$$s_3^{(n)} = \frac{3}{2} \left( 1 + \frac{1}{n-1} \right) \log l + \gamma, \quad (31)$$

in the large  $l$  limit. And the constant  $\gamma$  is

$$\begin{aligned} \gamma &= \frac{1}{(n-1)} \left( \frac{n}{2} \log \frac{\pi}{2} - \frac{3n}{2} \log \left( 2 + \frac{1}{\sqrt{S}} \right) - \right. \\ & \left. \log \Gamma(2n+1) + (2n+1) \log((n-1) \log S) \right). \end{aligned} \quad (32)$$

We find that the  $3/2$  in the log term of Rényi EE is universal which is similar as a central charge in CFT although the Motzkin is not a CFT. The constant term  $\gamma$  seems complex and non-universal.

## IV. NUMERICAL RESULT OF EE

Simulations of Rényi EE in quantum Monte Carlo methods have been well developed in recent years [33, 63–73]. Our simulation are based on the swap operator method in the above schemes. For pure states that can be written as the product states of two subsystems  $A$  and  $B$ , the  $\text{Swap}_A$  operator is defined as

$$\begin{aligned} & \text{Swap}_A \left( |A_1\rangle \otimes |B_1\rangle \right) \left( |A_2\rangle \otimes |B_2\rangle \right) \\ &= \left( |A_2\rangle \otimes |B_1\rangle \right) \left( |A_1\rangle \otimes |B_2\rangle \right). \end{aligned} \quad (33)$$

The ground state expected value of  $\text{Swap}_A$  operator is the 2nd order Rényi EE, and it can be sampled by Monte Carlo (MC) method [63, 68, 74],

$$s_A^{(2)} = -\log \text{Tr}(\rho_A^2) = -\log \langle \text{Swap}_A \rangle, \quad (34)$$

where  $\langle \dots \rangle$  indicates the expectation value of the two copies of the ground state,

$$|G\rangle^2 = |G\rangle \otimes |G\rangle. \quad (35)$$

Based on properties of the ground states of colored Motzkin chain, our algorithm can be simplified and the accuracy also be highly improved. The details of the algorithm are shown in the following.

### A. Detail of MC algorithm

The frustrated-free ground state is given in (5). Thus the expectation value of the  $\text{Swap}_A$  operator in (34) can be written as

$$\langle \text{Swap}_A \rangle = \sum_{i_1, i_2} \frac{1}{N} \langle G|^2 \text{Swap}_A |M_{i_1}\rangle \otimes |M_{i_2}\rangle. \quad (36)$$

Based on this formula, it is straight forward to setup a MC algorithm to estimate the second order Rényi EE  $s^{(2)}$ . One can simulate two replicas of configurations  $M_{i_1}$  and  $M_{i_2}$  with equal weights and measure the value of the estimator

$$\langle G|^2 \text{Swap} |M_{i_1}\rangle \otimes |M_{i_2}\rangle. \quad (37)$$

However, the symmetries of the colored Motzkin chain ground state allow us to further simplify the algorithm, so that only one replica is needed to sample. In this work, we consider the Motzkin chain of size  $2l$ , and are interested in the entanglement of the subsystem by cutting at the midpoint, thus all our discussions are constrained in the case  $A = l$ .

The swappability of Motzkin walks can be defined as follows. Exchanging half of the path of walks  $M_1$  and  $M_2$  bring us two new walks denoted as  $\tilde{M}_1$  and  $\tilde{M}_2$ . We assert that  $M_1$  is swappable to  $M_2$  if  $\tilde{M}_1$  also qualifies as a Motzkin walk. It is easy to identify the following properties of the Motzkin walks swappability: (1) If  $M_1$  is swappable with  $M_2$ , then  $M_2$  is also swappable with  $M_1$ ; (2) If  $M_1$  is swappable with  $M_2$ , and  $M_2$  is swappable with  $M_3$ , it follows that  $M_1$  is also swappable with  $M_3$ . Consequently, we can conclude that the measurement variable in equation (37) has only two possible values: it takes the value of one if  $M_{i_1}$  and  $M_{i_2}$  are swappable; otherwise, it takes the value of zero.

The colored Motzkin walks can then be categorized into classes  $c_m$  based on their swappability. In this context,  $m$  represents the height at the midpoint, which corresponds to the number of unpaired steps in half of the Motzkin walks. Notably, there are  $S^m$  equivalent classes, where the only distinction is the color permutation of the unpaired steps. Therefore, we group the  $S^m$  equivalent classes into a superclasses  $C_m$ . The relationship between the size of the superclass  $C_m$  represented as  $N_m$ , and the size of the class  $c_m$  represented as  $n_m$ , can be succinctly expressed by  $N_m = S^m n_m$ . With this understanding, we can simulate the distribution of  $C_m$ . The expected value  $\langle \text{Swap}_l \rangle$  can be estimated using the frequency  $\Lambda_m$  of each superclass  $C_m$ . And the second order Rényi EE is given with the formula:

$$s^{(2)} = -\log \sum_m S^{-m} \Lambda_m^2. \quad (38)$$

To estimate Rényi EE of other Rényi index, we usually generalize the Swap operator and  $n$  replicas need to be sampled. However, our algorithm can be directly generalized to simulate the Rényi EE of any Rényi index  $n$ , where  $n$  could be any positive real number and is not constrained to be an integer, using the following formula:

$$s^{(n)} = \frac{1}{1-n} \log \sum_{m=0}^l S^{-m(n-1)} \Lambda_m^n. \quad (39)$$

Additionally, this algorithm can be employed to determine the VN EE, which is given by:

$$s^{\text{VN}} = -\sum_{m=0}^l S^{-m(n-1)} \Lambda_m \log \Lambda_m. \quad (40)$$

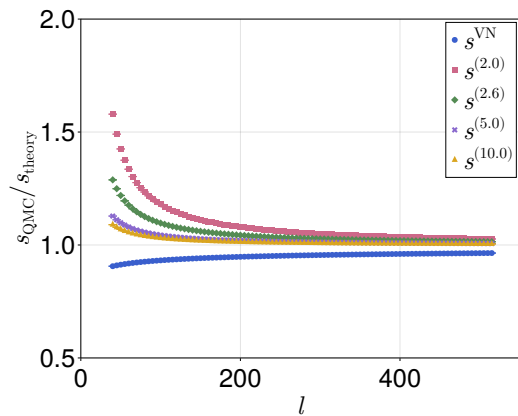


FIG. 2. The ratio of EE results from QMC and theory. The QMC are simulated on a two-color ( $S = 2$ ) Motzkin chain of size  $2l$ , and the EE are calculated on the subsystem by cutting at midpoint. As the subsystem size  $l$  increases, the the ratio tends to one. This shows our numerical and theoretical results agree well for large system size.

## B. Results of the EE from MC

VN EE and Rényi EE are computed by MC. Fig. 2 shows the ratio of our numerical results and the theoretical results for the EE, demonstrating a good agreement between them. The ratios converge to 1 while system size increases.

The MC data of the Motzkin chain were analyzed through a fitting process. We fitted the data using the form  $a\sqrt{l} + b \log l + \gamma$ , where  $a$  may either be zero or non-zero. Here,  $l$  represents the size of the subsystem, which is determined by making a cut at the midpoint of the chain. The results of  $a$  are presented in Fig. 3. For the VN EE, indicated by the point at  $n = 1$ , the numerical results closely align with the analytical predictions. Furthermore, our findings indicate that the square root term tends to diminish as  $n$  increases, consistent with the previous analysis that the Rényi EE does not include a  $\sqrt{l}$  term. Fig. 4 presents the results of  $b$  and  $\gamma$ , which further support the theoretical predictions.

We observe that there is an EE singularity of the Rényi index at  $n = 1$ , as indicated by both analytical and numerical results. The transition from a  $\log l$ -scaling to a  $\sqrt{l}$ -scaling is governed by the second term in the expansion of the Rényi entanglement entropy, as outlined in (10):

$$\begin{aligned} & \frac{1}{1-n} \log F_{2n}(p_1, p_2) \tilde{T}^{-n} \\ &= \frac{1}{1-n} \log F_{2n}(p_1, p_2) F_2^{-n}(p_1, 0). \end{aligned} \quad (41)$$

The exact value of  $F_{2n}(p_1, p_2) F_2^{-n}(p_1, 0)$  can be deter-

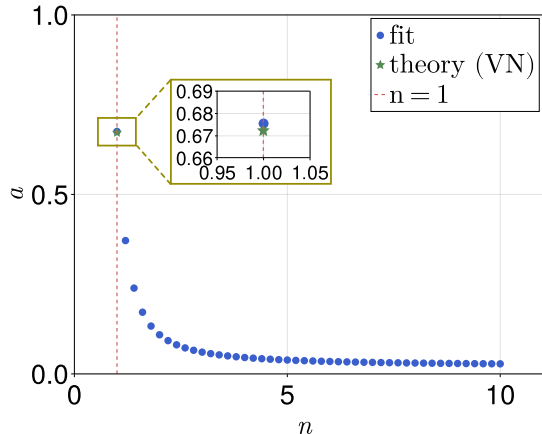


FIG. 3. The value of the coefficient of the  $\sqrt{l}$  term  $a$  in EE for a 2-colored ( $S = 2$ ) Motzkin chain. The fitting results are illustrated as blue dots, which are fitted with the form:  $a\sqrt{l} + b \log l + \gamma$ , where  $l$  is the subsystem size. The theory prediction for VN EE is also shown as a green star. The QMC are sampled on system size from 80 to 1230 sites.

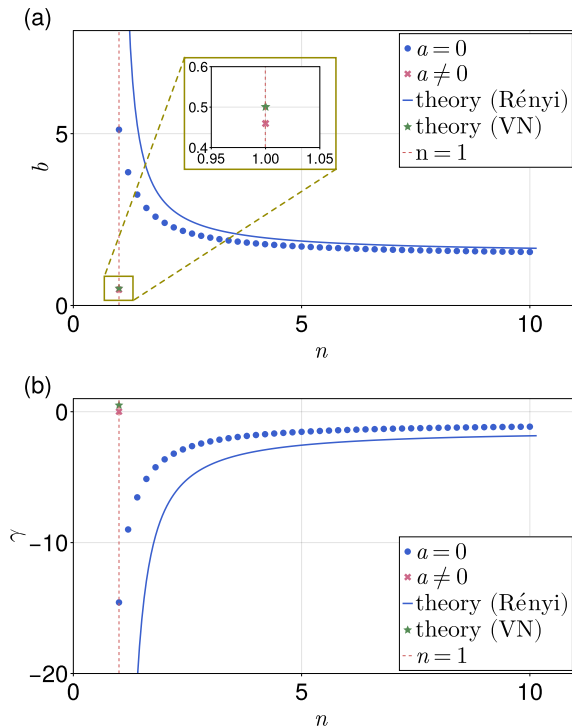


FIG. 4. The value of coefficients in the scaling form of Rényi and VN EE for a 2-colored Motzkin chain. The QMC are sampled on the system sizes from 80 to 1260 sites. The EE data are fitted within the form  $b \log l + \gamma$ , represented by the blue dots. VN EE data are also fitted within the form  $a\sqrt{l} + b \log l + \gamma$ , represented by the pink crosses. The theory predictions are also shown, respectively. The QMC are sampled on the system sizes from 80 to 1230 sites. (a) Value of  $b$ , the coefficient of the  $\log l$  term. (b) The constant term  $\gamma$ .

mined in specific values of  $n$  and  $S$ . For the colorless Motzkin chain,  $p_2 = 0$ , and it can be proved that  $F_{2n}(p_1, p_2)F_2^{-n}(p_1, 0) > 1$  and has an upper bound in the large  $l$  limit. Thus equation (41) contributes a constant term to the scaling of EE. For the case  $S > 1$ , however, the value of  $F_{2n}(p_1, p_2)F_2^{-n}(p_1, 0)$  can be determined in specific values of  $(n-1)\sqrt{l}$  in the large  $l$  limit. It can be summarized as

$$F_{2n}\tilde{T}^{-n} = \begin{cases} 0, & (n-1)\sqrt{l} \rightarrow +\infty \\ 1, & (n-1)\sqrt{l} \rightarrow 0^+. \end{cases} \quad (42)$$

When analyzing the scaling of the Rényi EE, we will consider the limit  $(n-1)\sqrt{l} \rightarrow \infty$ . However, this term is treated as zero for the VN EE case. It reflects that the limits of  $l \rightarrow \infty$  and  $n \rightarrow 1$  do not commute in the EE calculation.

As  $n = 1$  (the von Neumann EE) is the EE singularity of an infinite Motzkin spin chain, the finite-size modification becomes significantly large near  $n = 1$ . This finite-size effect is dominated by the term  $\frac{1}{(n-1)\sqrt{l}}$ , which accounts for the considerable difference observed between the analytical results and the numerical results shown in Fig. 4 as  $n$  approaches one.

From the perspective of the entanglement spectrum, the differing scaling behaviors of the von Neumann (VN) entanglement entropy (EE) and the Rényi EE arise from the abundance of highly excited levels. Entanglement entropies can be understood as thermal entropies of an entanglement Hamiltonian  $H_E$ . The entanglement spectrum is the eigenvalues of entanglement Hamiltonian [75–77]. For any given Rényi index, the Rényi EE exhibits the same scaling and is solely dependent on the lowest level in the spectrum. In contrast, the large number of high excited levels—as shown in Fig. 5—causes the VN EE to demonstrate a larger scaling behavior than the Rényi EE.

## V. DISORDER OPERATOR

The disorder operator [78–87] is a non-local operator capable of detecting higher-form symmetries, which are often challenging to measure using local operators. For a system with global symmetry, the DO is defined as the symmetry operator that acts on a specific subsystem. Recent research [88–93] has demonstrated that the DO exhibits universal scaling behavior across various quantum systems. Typically, the scaling behavior of the minus of logarithmic DO is similar to the scaling behavior of entanglement entropy, which captures essential information from CFT.

The Hamiltonian and ground state of colored Motzkin chain possess multiple symmetries [94]. Firstly, the colored Motzkin chain has continuous  $U(1)$  symmetry characterized by the charge  $Q^z = \sum_j^{2l} S_j^z$ , where  $2l$  is the

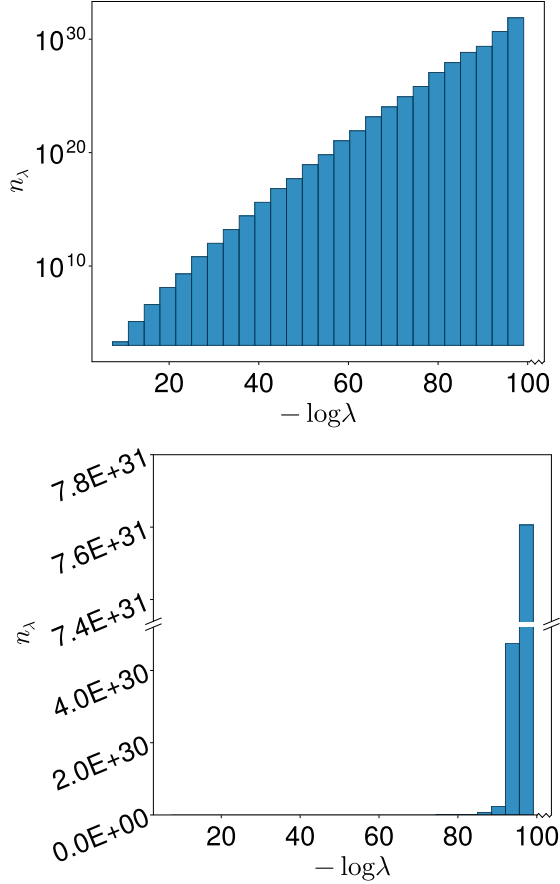


FIG. 5. The density of states in the entanglement spectrum, obtained by the reduced density matrix of a spin-2 chain of length 1070. The horizontal axis  $-\log\lambda$  is the eigenvalue of the entanglement Hamiltonian ( $\lambda$  is the eigenvalue of the reduced density matrix), the vertical axis is the density of states in a small window of  $-\log\lambda$  (logarithmic/natural scale in the upper/bottom figure).

system size. Consequently, we can define the DO as

$$X^z(\theta) = \prod_j^l e^{i\theta S_j^z}, \quad (43)$$

which acts solely on half of the chain obtained by cutting at the midpoint. The average of DO is then given by

$$\langle X^z(\theta) \rangle = \sum_{m=0}^l \lambda_m \left( \sum_{k=1}^S e^{ik\theta} \right)^m. \quad (44)$$

By substituting (8) into (44), setting  $\xi = \frac{m}{\sqrt{l}}$ , and utilizing the integral approximation, we obtain the following

expression of DO:

$$\langle X^z(\theta) \rangle = \frac{1}{\sqrt{l\tilde{T}}} \int_0^\infty d\xi \sqrt{l} \xi^2 e^{-p_1(1,S)\xi^2} \times \left( \frac{\sin S\frac{\theta}{2}}{S \sin \frac{\theta}{2}} \right)^{\sqrt{l}\xi} e^{-i\frac{S+1}{2}\theta\sqrt{l}\xi}, \quad (45)$$

where  $\tilde{T}$  is defined in (23). Define the following functions

$$\chi_\alpha(S, \theta, l) = \int_0^\infty d\xi \xi^\alpha e^{-p_1(1,S)\xi^2} \times \left( \frac{\sin S\frac{\theta}{2}}{S \sin \frac{\theta}{2}} \right)^{\sqrt{l}\xi} e^{i\frac{S+1}{2}\theta\sqrt{l}\xi}, \quad (46)$$

$$y(S, \theta) = \log \left( \frac{\sin S\frac{\theta}{2}}{S \sin \frac{\theta}{2}} \right) + i\frac{S+1}{2}\theta. \quad (47)$$

It is easy to prove the following relations:

$$\begin{aligned} \frac{d}{dl} \chi_\alpha &= \frac{1}{2\sqrt{l}} y \chi_{\alpha+1}, \\ \chi_\alpha &= -\frac{\sqrt{l}}{\alpha+1} y \chi_{\alpha+1} + 2p_1(1, S) \chi_{\alpha+2}, \end{aligned} \quad (48)$$

and the DO can be expressed as  $\langle X^z(\theta) \rangle = \chi_2$ . It is noteworthy that term  $e^{-p_1(1,S)\xi^2}$  significantly suppress the contribution from large  $\xi$  in the integral in (46). Thus we have the inequality  $|\chi_{\alpha_1}| > |\chi_{\alpha_2}|$  if  $\alpha_1 < \alpha_2$ . Using the these relations, we can calculate the limit,

$$\lim_{l \rightarrow \infty} \frac{-\log |\langle X^z(\theta) \rangle|}{\log l} = \frac{3}{2}. \quad (49)$$

Therefore, the scaling behavior of the minus of logarithmic DO can be expressed as:

$$-\log |\langle X^z(\theta) \rangle| = \frac{3}{2} \log l + const. \quad (50)$$

Note that the result holds for both colorless and colored case. The universal coefficient of log term is  $3/2$ , same as in Rényi EE.

We calculated the DO numerically using MC simulations, and the results of the  $S = 1, 2, 3$  cases are presented in Fig. 6. It shows the logarithmic scaling is agreed well with the theoretical result in (50). The fitting results of  $b$  are shown in Fig. 7, which are obtained by fitting the DO to the function  $b \log l + const.$  using data from different segments of system size. It shows as the system size increases  $b$  approaches  $3/2$ .

In addition to the  $U(1)$  symmetry above, the ground state of the Motzkin chain exhibits an additional

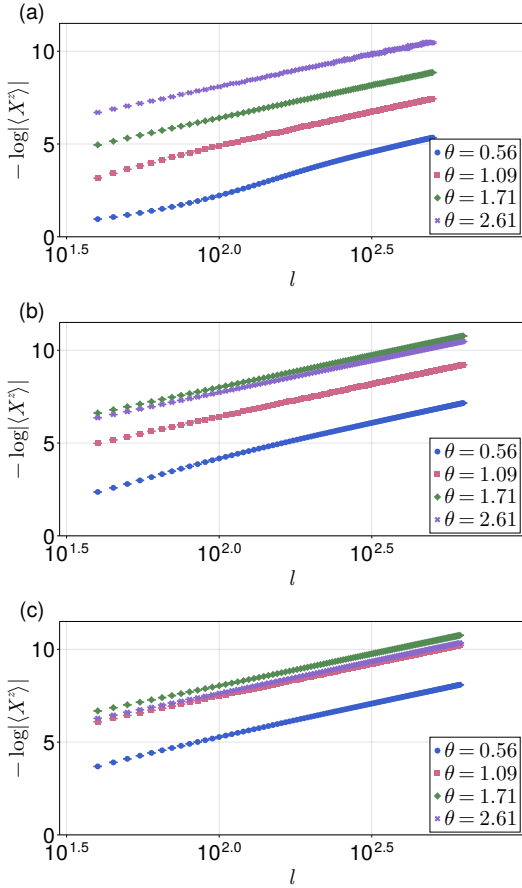


FIG. 6. The minus of logarithmic DO under  $U(1)$  symmetry with charge  $Q^z$ . The system is a 2-colored Motzkin chain with size  $2l$ , and the QMC are sampled on system size ranging from 80 to 1230 sites. The horizontal axis is the subsystem size  $l$ , by cutting at the midpoint of the chain. (a) Colorless Motzkin chain. (b) 2-colored Motzkin chain. (c) 3-colored Motzkin chain.

$U(1)$  symmetry characterized by the charge  $Q^c = \sum_j^{2l} \sum_k^S (|\uparrow^k\rangle_j \langle \uparrow^k| - |\downarrow^k\rangle_j \langle \downarrow^k|)$ . Then the DO is:

$$\begin{aligned} X^c(\theta) &= \left\langle \prod_j^l e^{i\theta \sum_k^S (|\uparrow^k\rangle_j \langle \uparrow^k| - |\downarrow^k\rangle_j \langle \downarrow^k|)} \right\rangle \\ &= \frac{1}{T} \sum_{m=0}^l \frac{m^2}{l} e^{-p_1(1,S) \frac{m^2}{l}} e^{ikm\theta}, \end{aligned} \quad (51)$$

In the limit as  $l \rightarrow \infty$ , the scaling behavior of the minus of logarithmic DO is also given by  $\log l$ ,

$$-\log |\langle X^c(\theta) \rangle| = \frac{3}{2} \log l + const. \quad (52)$$

The numerical results are illustrated in Fig. 8.(a).

The model also has a permutation symmetry concerning different colors. Take the example in Fig. 1 for instance, it is still a Motzkin walk after exchanging the blue

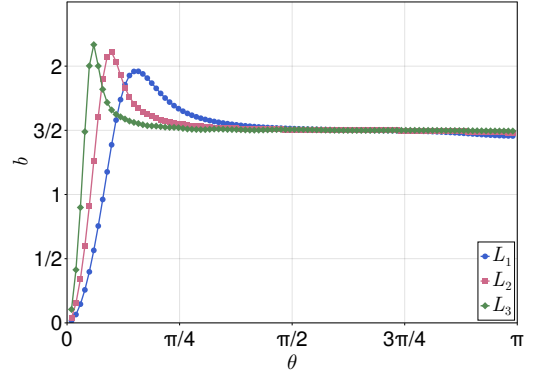


FIG. 7. The value of  $b$  by fitting the data of  $-\log |\langle X^z(\theta) \rangle|$  within the form  $b \log l + const.$  The horizontal axis represents the phase  $\theta$  in the  $U(1)$  symmetry. Different colors correspond to various system size segments. Specifically,  $L_1$  are system sizes ranging from 80 to 310 sites,  $L_2$  are from 300 to 530 sites and  $L_3$  are from 1020 to 1260 sites. The DOs are calculated on subsystems obtained by cutting at the chain at the midpoint. The figure demonstrates that as the system size increases  $b$  approaches  $3/2$ , which is consistent with our analytical predictions.

and pink steps. We introduce a DO  $X^p$  that permutes the colors within the subsystems. It can be proved that the expectation value of this DO equals  $\lambda_0$  as outlined in (8), which can be estimated in large  $l$  limit as:

$$\begin{aligned} \langle X^p \rangle &= \lambda_0 = \frac{1}{T} \left( \sum_{i=0}^{l/2} S^i \frac{l!}{(i+1)!i!(l-2i)!} \right)^2 \\ &\propto \frac{1}{T} (2\sqrt{S} + 1)^{2n} n^{-4} \\ &\propto n^{-3/2}. \end{aligned} \quad (53)$$

Consequently, the minus of logarithmic DO exhibits logarithmic scaling expressed as:

$$-\log |\langle X^p \rangle| = \frac{3}{2} \log l + const. \quad (54)$$

The numerical results that support these findings are presented in Fig. 8.(b).

In summary, we investigated the scaling behavior of three different disorder operators, based on different symmetries of the ground states in both the colorless and colored cases. Our analysis and numerical results indicate that the scaling of the DOs follow a logarithmic form. Furthermore, we observe that all the coefficients preceding  $\log l$  are consistently equal to  $3/2$  under different symmetries, regardless of whether it is colored or colorless. This universal constant also appears in the Rényi EE of the colored case in (32).



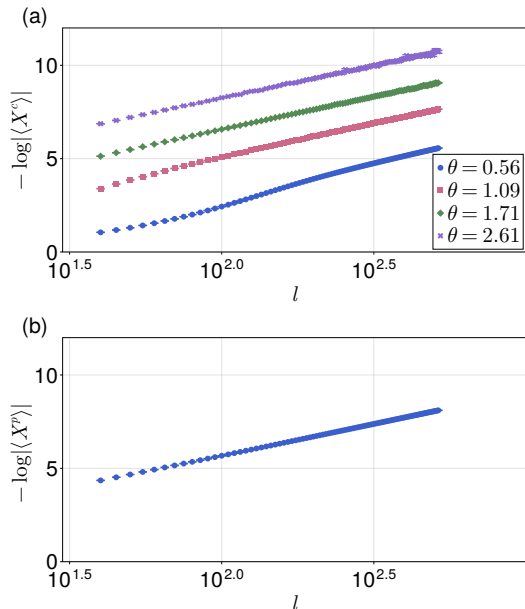


FIG. 8. The minus of logarithmic DO. The system is a 2-colored Motzkin chain, and the QMC are sampled on system size ranging from 80 to 1230 sites. The horizontal axis is the subsystem size  $l$ , by cutting at the midpoint of the chain. (a) DO of  $U(1)$  symmetry with charge  $Q^c$ . (b) DO of permutation symmetry.

## VI. SUMMARY AND DISCUSSION

It has always been believed that the von Neumann entanglement entropy could be obtained through the analytic continuation of the Rényi index from Rényi entropy. However, the colored Motzkin chain serves as a counterexample, as the expression for the leading term of Rényi entanglement entropy diverges at  $n = 1$  and has to in-

roduce an extra term for correction. We investigate the scaling behaviors of EE theoretically and numerically to demonstrate the failure of analytic continuation. Mathematically, this singularity is because the limits  $l \rightarrow \infty$  and  $n \rightarrow 1$  can not commute in the derivation procedures of von Neumann and Rényi entanglement entropies respectively. On the other hand, it also could be understood by the exponential increasing density of states in its entanglement spectrum.

We have also explored the scaling of logarithmic disorder operators under different symmetries in the colored Motzkin chains theoretically and numerically. The theoretical analysis predicts that all the logarithmic DOs exhibit same scaling as Rényi EE. Our numerical simulations also confirm the theoretical calculations. The scaling of the von Neumann EE, Rényi EE and the logarithmic DOs point out that the coefficient of the  $\log l$  term is a universal fingerprint to identify the physics of

Motzkin walks.

Although the entanglement entropy is difficult to measure in experiments, even in a small system [95, 96], the disorder operator is an observable that can be easily extracted particularly in cold atom platforms. We propose to probe the constrained physics of Motzkin systems intrinsically via disorder operators experimentally.

## VII. ACKNOWLEDGMENT.-

We thank the helpful discussions with Meng Cheng and Zi Hong Liu. ZL and ZY acknowledge the start-up funding of Westlake University. Zenan Liu thanks the China Postdoctoral Science Foundation under Grants No.2024M762935 and NSFC Special Fund for Theoretical Physics under Grants No.12447119. The authors thank the high-performance computing center of Westlake University and the Beijing PARATERA Tech Co.,Ltd. for providing HPC resources.

- 
- [1] L. Amico, R. Fazio, A. Osterloh, and V. Vedral, Entanglement in many-body systems, *Rev. Mod. Phys.* **80**, 517 (2008).
  - [2] N. Laflorencie, Quantum entanglement in condensed matter systems, *Physics Reports* **646**, 1 (2016), quantum entanglement in condensed matter systems.
  - [3] B. Zeng, X. Chen, D.-L. Zhou, X.-G. Wen, *et al.*, *Quantum information meets quantum matter* (Springer, 2019).
  - [4] M. A. Nielsen and I. L. Chuang, *Quantum computation and quantum information* (Cambridge university press, 2010).
  - [5] M. M. Wilde, *Quantum information theory* (Cambridge university press, 2013).
  - [6] A. Kitaev and J. Preskill, Topological entanglement entropy, *Phys. Rev. Lett.* **96**, 110404 (2006).
  - [7] M. Levin and X.-G. Wen, Detecting topological order in a ground state wave function, *Phys. Rev. Lett.* **96**, 110405 (2006).
  - [8] G. Vidal, J. I. Latorre, E. Rico, and A. Kitaev, Entanglement in quantum critical phenomena, *Physical Review Letters* **90**, 227902 (2003).
  - [9] V. E. Korepin, Universality of entropy scaling in one dimensional gapless models, *Phys. Rev. Lett.* **92**, 096402 (2004).
  - [10] Z. Wang, Z. Deng, Z. Wang, Y.-M. Ding, W. Guo, and Z. Yan, Probing phase transition and underlying symmetry breaking via entanglement entropy scanning, arXiv

- preprint arXiv:2409.09942 (2024).
- [11] P. Calabrese and A. Lefevre, Entanglement spectrum in one-dimensional systems, *Phys. Rev. A* **78**, 032329 (2008).
- [12] E. Fradkin and J. E. Moore, Entanglement entropy of 2d conformal quantum critical points: Hearing the shape of a quantum drum, *Phys. Rev. Lett.* **97**, 050404 (2006).
- [13] Z. Nussinov and G. Ortiz, Sufficient symmetry conditions for topological quantum order, *Proc. Nat. Acad. Sci.* **106**, 16944 (2009).
- [14] Z. Nussinov and G. Ortiz, A symmetry principle for topological quantum order, *Annals Phys.* **324**, 977 (2009).
- [15] H. Casini and M. Huerta, Universal terms for the entanglement entropy in 2+1 dimensions, *Nucl. Phys. B* **764**, 183 (2007), arXiv:hep-th/0606256.
- [16] W. Ji and X.-G. Wen, Noninvertible anomalies and mapping-class-group transformation of anomalous partition functions, *Phys. Rev. Research* **1**, 033054 (2019).
- [17] W. Ji and X.-G. Wen, Categorical symmetry and noninvertible anomaly in symmetry-breaking and topological phase transitions, *Phys. Rev. Research* **2**, 033417 (2020).
- [18] L. Kong, T. Lan, X.-G. Wen, Z.-H. Zhang, and H. Zheng, Algebraic higher symmetry and categorical symmetry: A holographic and entanglement view of symmetry, *Phys. Rev. Research* **2**, 043086 (2020).
- [19] X.-C. Wu, W. Ji, and C. Xu, Categorical symmetries at criticality, *Journal of Statistical Mechanics: Theory and Experiment* **2021**, 073101 (2021).
- [20] W. Ding, N. E. Bonesteel, and K. Yang, Block entanglement entropy of ground states with long-range magnetic order, *Physical Review A* **77**, 052109 (2008).
- [21] Q.-C. Tang and W. Zhu, Critical scaling behaviors of entanglement spectra, *Chinese Physics Letters* **37**, 010301 (2020).
- [22] J. Zhao, Z. Yan, M. Cheng, and Z. Y. Meng, Higher-form symmetry breaking at ising transitions, *Phys. Rev. Research* **3**, 033024 (2021).
- [23] X.-C. Wu, C.-M. Jian, and C. Xu, Universal features of higher-form symmetries at phase transitions, *SciPost Phys.* **11**, 33 (2021).
- [24] J. Zhao, Y.-C. Wang, Z. Yan, M. Cheng, and Z. Y. Meng, Scaling of entanglement entropy at deconfined quantum criticality, *Physical Review Letters* **128**, 010601 (2022).
- [25] B.-B. Chen, H.-H. Tu, Z. Y. Meng, and M. Cheng, Topological disorder parameter: A many-body invariant to characterize gapped quantum phases, *Phys. Rev. B* **106**, 094415 (2022).
- [26] J. Zhao, B.-B. Chen, Y.-C. Wang, Z. Yan, M. Cheng, and Z. Y. Meng, Measuring rényi entanglement entropy with high efficiency and precision in quantum monte carlo simulations, *npj Quantum Materials* **7**, 69 (2022).
- [27] Z. Yan and Z. Y. Meng, Unlocking the general relationship between energy and entanglement spectra via the wormhole effect, *Nature Communications* **14**, 2360 (2023).
- [28] P. Calabrese and J. Cardy, Entanglement entropy and quantum field theory, *Journal of Statistical Mechanics: Theory and Experiment* **2004**, P06002 (2004).
- [29] Y.-M. Ding, Y. Tang, Z. Wang, Z. Wang, B.-B. Mao, and Z. Yan, Tracking the variation of entanglement rényi negativity: an efficient quantum monte carlo method (2024), arXiv:2409.10273 [cond-mat.str-el].
- [30] M. A. Metlitski and T. Grover, Entanglement entropy of systems with spontaneously broken continuous symmetry, arXiv e-prints, arXiv:1112.5166 (2011), arXiv:1112.5166 [cond-mat.str-el].
- [31] Z. Deng, L. Liu, W. Guo, and H. Lin, Improved scaling of the entanglement entropy of quantum antiferromagnetic heisenberg systems, *Physical Review B* **108**, 125144 (2023).
- [32] Z. Deng, L. Liu, W. Guo, and H.-q. Lin, Diagnosing  $so(5)$  symmetry and first-order transition in the  $j - q_3$  model via entanglement entropy, arXiv preprint arXiv:2401.12838 (2024).
- [33] Z. Wang, Z. Wang, Y.-M. Ding, B.-B. Mao, and Z. Yan, Bipartite reweight-annealing algorithm to extract large-scale data of entanglement entropy and its derivative in high precision (2024), arXiv:2406.05324 [cond-mat.str-el].
- [34] T. Grover, Y. Zhang, and A. Vishwanath, Entanglement entropy as a portal to the physics of quantum spin liquids, *New Journal of Physics* **15**, 025002 (2013).
- [35] M. Nozaki, T. Numasawa, and T. Takayanagi, Quantum entanglement of local operators in conformal field theories, *Physical review letters* **112**, 111602 (2014).
- [36] J. Cardy and E. Tonni, Entanglement hamiltonians in two-dimensional conformal field theory, *Journal of Statistical Mechanics: Theory and Experiment* **2016**, 123103 (2016).
- [37] P. Bueno, R. C. Myers, and W. Witczak-Krempa, Universality of corner entanglement in conformal field theories, *Physical review letters* **115**, 021602 (2015).
- [38] H. Casini and M. Huerta, Positivity, entanglement entropy, and minimal surfaces, *Journal of High Energy Physics* **2012**, 87 (2012).
- [39] R. Longo and F. Xu, Von neumann entropy in qft, *Communications in Mathematical Physics* **381**, 1031 (2021).
- [40] P. Boes, J. Eisert, R. Gallego, M. P. Müller, and H. Wilming, Von neumann entropy from unitarity, *Physical review letters* **122**, 210402 (2019).
- [41] F. Giraldi and P. Grigolini, Quantum entanglement and entropy, *Physical Review A* **64**, 032310 (2001).
- [42] W. Donnelly, Decomposition of entanglement entropy in lattice gauge theory, *Physical Review D—Particles, Fields, Gravitation, and Cosmology* **85**, 085004 (2012).
- [43] T. Cubitt, A. W. Harrow, D. Leung, A. Montanaro, and A. Winter, Counterexamples to additivity of minimum output p-renyi entropy for p close to 0, *Communications in mathematical physics* **284**, 281 (2008).
- [44] G. Camilo, G. T. Landi, and S. Eliëns, Strong subadditivity of the rényi entropies for bosonic and fermionic gaussian states, *Phys. Rev. B* **99**, 045155 (2019).
- [45] B. Collins and I. Nechita, Random quantum channels ii: Entanglement of random subspaces, rényi entropy estimates and additivity problems, *Advances in Mathematics* **226**, 1181 (2011).
- [46] E. D’Hoker, X. Dong, and C.-H. Wu, An alternative method for extracting the von neumann entropy from rényi entropies, *Journal of High Energy Physics* **2021**, 1 (2021).
- [47] J. Fuentes and J. Gonçalves, Rényi entropy in statistical mechanics, *Entropy* **24**, 1080 (2022).
- [48] J. Eisert, M. Cramer, and M. B. Plenio, *Colloquium* : Area laws for the entanglement entropy, *Reviews of Modern Physics* **82**, 277 (2010).

- [49] S. T. Flammia, A. Hamma, T. L. Hughes, and X.-G. Wen, Topological Entanglement Rényi Entropy and Reduced Density Matrix Structure, *Physical Review Letters* **103**, 261601 (2009).
- [50] X.-C. Wu, C.-M. Jian, and C. Xu, Universal features of higher-form symmetries at phase transitions, *SciPost Phys.* **11**, 033 (2021).
- [51] E. Lake, Higher-form symmetries and spontaneous symmetry breaking, arXiv:1802.07747.
- [52] E. Fradkin, Disorder operators and their descendants, *J. Stat. Phys.* **167**, 427 (2017).
- [53] Z. Liu, R.-Z. Huang, Y.-C. Wang, Z. Yan, and D.-X. Yao, Measuring the boundary gapless state and criticality via disorder operator, *Phys. Rev. Lett.* **132**, 206502 (2024).
- [54] J. Zhao, Z. Yan, M. Cheng, and Z. Y. Meng, Higher-form symmetry breaking at ising transitions, *Phys. Rev. Res.* **3**, 033024 (2021).
- [55] Y.-C. Wang, M. Cheng, and Z. Y. Meng, Scaling of the disorder operator at  $(2+1)d$  u(1) quantum criticality, *Phys. Rev. B* **104**, L081109 (2021).
- [56] Y.-C. Wang, N. Ma, M. Cheng, and Z. Y. Meng, Scaling of the disorder operator at deconfined quantum criticality, *SciPost Phys.* **13**, 123 (2022).
- [57] W. Jiang, B.-B. Chen, Z. H. Liu, J. Rong, F. F. Assaad, M. Cheng, K. Sun, and Z. Y. Meng, Many versus one: The disorder operator and entanglement entropy in fermionic quantum matter, *SciPost Phys.* **15**, 082 (2023).
- [58] Z. H. Liu, W. Jiang, B.-B. Chen, J. Rong, M. Cheng, K. Sun, Z. Y. Meng, and F. F. Assaad, Fermion disorder operator at gross-neveu and deconfined quantum criticalities, *Phys. Rev. Lett.* **130**, 266501 (2023).
- [59] Z. H. Liu, Y. Da Liao, G. Pan, M. Song, J. Zhao, W. Jiang, C.-M. Jian, Y.-Z. You, F. F. Assaad, Z. Y. Meng, and C. Xu, Disorder operator and rényi entanglement entropy of symmetric mass generation, *Phys. Rev. Lett.* **132**, 156503 (2024).
- [60] S. Bravyi, L. Caha, R. Movassagh, D. Nagaj, and P. W. Shor, Criticality without frustration for quantum spin-1 chains, *Physical Review Letters* **109**, 207202 (2012).
- [61] R. Movassagh and P. W. Shor, Supercritical entanglement in local systems: Counterexample to the area law for quantum matter, *Proceedings of the National Academy of Sciences* **113**, 13278 (2016), <https://www.pnas.org/doi/pdf/10.1073/pnas.1605716113>.
- [62] F. Sugino and V. Korepin, Rényi entropy of highly entangled spin chains, *Int. J. Mod. Phys. B* **32**, 1850306 (2018), arXiv:1806.04049 [hep-th].
- [63] M. B. Hastings, I. González, A. B. Kallin, and R. G. Melko, Measuring renyi entanglement entropy in quantum monte carlo simulations, *Physical Review Letters* **104**, 157201 (2010), arXiv:1001.2335 [cond-mat.str-el].
- [64] S. Humeniuk and T. Roscilde, Quantum monte carlo calculation of entanglement rényi entropies for generic quantum systems, *Physical Review B* **86**, 235116 (2012), arXiv:1203.5752 [cond-mat.str-el].
- [65] S. Inglis and R. G. Melko, Wang-landau method for calculating rényi entropies in finite-temperature quantum monte carlo simulations, *Physical Review E* **87**, 013306 (2013).
- [66] P. Broecker and S. Trebst, Rényi entropies of interacting fermions from determinantal quantum monte carlo simulations, *Journal of Statistical Mechanics: Theory and Experiment* **2014**, P08015 (2014).
- [67] D. J. Luitz, X. Plat, N. Laflorencie, and F. Alet, Improving entanglement and thermodynamic rényi entropy measurements in quantum monte carlo, *Physical Review B* **90**, 125105 (2014).
- [68] J. Pei, S. Han, H. Liao, and T. Li, The rényi entanglement entropy of a general quantum dimer model at the RK point: A highly efficient algorithm, *Journal of Physics: Condensed Matter* **26**, 035601 (2014).
- [69] L. Wang and M. Troyer, Renyi entanglement entropy of interacting fermions calculated using the continuous-time quantum monte carlo method, *Physical Review Letters* **113**, 110401 (2014).
- [70] F. F. Assaad, Stable quantum monte carlo simulations for entanglement spectra of interacting fermions, *Physical Review B* **91**, 125146 (2015).
- [71] J. D’Emidio, Entanglement entropy from nonequilibrium work, *Physical Review Letters* **124**, 110602 (2020), arXiv:1904.05918 [cond-mat.str-el].
- [72] J. Zhao, B.-B. Chen, Y.-C. Wang, Z. Yan, M. Cheng, and Z. Y. Meng, Measuring rényi entanglement entropy with high efficiency and precision in quantum monte carlo simulations, *npj Quantum Materials* **7**, 69 (2022), arXiv:2112.15178 [cond-mat.str-el].
- [73] Z. Yan and Z. Y. Meng, Unlocking the general relationship between energy and entanglement spectra via the wormhole effect, *Nature Communications* **14**, 2360 (2023), arXiv:2112.05886 [cond-mat.str-el].
- [74] X. Zhou, Z. Y. Meng, Y. Qi, and Y. Da Liao, Incremental SWAP operator for entanglement entropy: Application for exponential observables in quantum monte carlo simulation, *Phys. Rev. B* **109**, 165106 (2024), arXiv:2401.07244 [cond-mat.str-el].
- [75] Z. Yan and Z. Y. Meng, Unlocking the general relationship between energy and entanglement spectra via the wormhole effect, *Nature Communications* **14**, 2360 (2023).
- [76] Z. Liu, R.-Z. Huang, Z. Yan, and D.-X. Yao, Demonstrating the wormhole mechanism of the entanglement spectrum via a perturbed boundary, *Physical Review B* **109**, 094416 (2024).
- [77] C. Li, R.-Z. Huang, Y.-M. Ding, Z. Y. Meng, Y.-C. Wang, and Z. Yan, Relevant long-range interaction of the entanglement hamiltonian emerges from a short-range gapped system, *Physical Review B* **109**, 195169 (2024).
- [78] L. P. Kadanoff and H. Ceva, Determination of an operator algebra for the two-dimensional ising model, *Physical Review B* **3**, 3918 (1971).
- [79] F. J. Wegner, Duality in Generalized Ising Models and Phase Transitions without Local Order Parameters, *Journal of Mathematical Physics* **12**, 2259 (1971).
- [80] E. Fradkin and L. Susskind, Order and disorder in gauge systems and magnets, *Physical Review D* **17**, 2637 (1978).
- [81] Z. Nussinov and G. Ortiz, A symmetry principle for topological quantum order, *Annals of Physics* **324**, 977 (2009).
- [82] A. Kapustin and N. Seiberg, Coupling a QFT to a TQFT and duality, *Journal of High Energy Physics* **2014**, 1 (2014).
- [83] D. Gaiotto, A. Kapustin, N. Seiberg, and B. Willett, Generalized global symmetries, *Journal of High Energy Physics* **2015**, 172 (2015).
- [84] E. Fradkin, Disorder operators and their descendants, *Journal of Statistical Physics* **167**, 427 (2017),

- arXiv:1610.05780 [cond-mat.stat-mech].
- [85] X.-G. Wen, *Colloquium* : Zoo of quantum-topological phases of matter, *Reviews of Modern Physics* **89**, 041004 (2017).
- [86] X.-G. Wen, Choreographed entanglement dances: Topological states of quantum matter, *Science* **363**, eaal3099 (2019).
- [87] W. Ji and X.-G. Wen, Categorical symmetry and noninvertible anomaly in symmetry-breaking and topological phase transitions, *Physical Review Research* **2**, 033417 (2020), arXiv:1912.13492 [cond-mat.str-el].
- [88] W. Witczak-Krempa, Entanglement susceptibilities and universal geometric entanglement entropy, *Phys. Rev. B* **99**, 075138 (2019), arXiv:1810.07209 [cond-mat.str-el].
- [89] L. Kong, T. Lan, X.-G. Wen, Z.-H. Zhang, and H. Zheng, Algebraic higher symmetry and categorical symmetry: A holographic and entanglement view of symmetry, *Physical Review Research* **2**, 043086 (2020).
- [90] X.-C. Wu, W. Ji, and C. Xu, Categorical symmetries at criticality, *Journal of Statistical Mechanics: Theory and Experiment* **2021**, 073101 (2021), arXiv:2012.03976 [cond-mat.str-el].
- [91] J. Zhao, Z. Yan, M. Cheng, and Z. Y. Meng, Higher-form symmetry breaking at ising transitions, *Physical Review Research* **3**, 033024 (2021), arXiv:2011.12543 [cond-mat.str-el].
- [92] Y.-C. Wang, M. Cheng, and Z. Y. Meng, Scaling of disorder operator at  $(2+1)d$   $U(1)$  quantum criticality, *Physical Review B* **104**, 081109 (2021), arXiv:2101.10358 [cond-mat.str-el].
- [93] W. Jiang, B.-B. Chen, Z. H. Liu, J. Rong, F. F. Asaad, M. Cheng, K. Sun, and Z. Y. Meng, Many versus one: The disorder operator and entanglement entropy in fermionic quantum matter, *SciPost Phys.* **15**, 082 (2023), arXiv:2209.07103 [cond-mat.str-el].
- [94] V. Menon, A. Gu, and R. Movassagh, Symmetries, correlation functions, and entanglement of general quantum motzkin spin-chains, *ArXiv e-prints* (2024), arXiv:2408.16070 [quant-ph].
- [95] R. Islam, R. Ma, P. M. Preiss, M. Eric Tai, A. Lukin, M. Rispoli, and M. Greiner, Measuring entanglement entropy in a quantum many-body system, *Nature* **528**, 77 (2015).
- [96] D. A. Abanin and E. Demler, Measuring entanglement entropy of a generic many-body system with a quantum switch, *Phys. Rev. Lett.* **109**, 020504 (2012).